



Excitons and carriers in transient absorption and time-resolved ARPES spectroscopy: An *ab initio* approach

D. Sangalli 

Istituto di Struttura della Materia of the National Research Council, Via Salaria Km 29.3, I-00016 Montelibretti, Italy and European Theoretical Spectroscopy Facilities (ETSF)

 (Received 4 June 2021; accepted 5 August 2021; published 20 August 2021)

I present a fully *ab initio* scheme to model transient spectroscopy signals in the presence of strongly bound excitons. Using LiF as a prototype material, I show that the scheme is able to capture the exciton signature both in time-resolved angle-resolved photoemission spectroscopy and transient absorption experiments. The approach is completely general and can become the reference scheme for modeling pump and probe experiment in a wide range of materials.

DOI: [10.1103/PhysRevMaterials.5.083803](https://doi.org/10.1103/PhysRevMaterials.5.083803)

I. INTRODUCTION

The exciton is a quasiparticle composed by an electron-hole pair bound via Coulomb interaction [1]. In condensed matter physics, exciton energies, $\omega_{\lambda\mathbf{q}}$, and wave functions, $A^{\lambda\mathbf{q}}$, are obtained via the solution of the *ab initio* Bethe-Salpeter equation (BSE), and well describe the neutral excitations of materials in the linear response regime [2,3]. Indeed the energy difference between the electronic ground state, $|\Psi_0^N\rangle$, and the neutral excited state, $|\Psi_I^N\rangle$, is well approximated by $\omega_{\lambda\mathbf{q}} \approx (E_I^N - E_0^N)$. Similarly the many-body wave function can be approximated as $|\Psi_I^N\rangle \approx \hat{e}_{\lambda\mathbf{q}}^\dagger |\Psi_0^N\rangle$, via the definition of the exciton creation operator $\hat{e}_{\lambda\mathbf{q}}^\dagger = \sum_{c\nu\mathbf{k}} A_{c\nu\mathbf{k}}^{\lambda\mathbf{q}} \hat{a}_{c\mathbf{k}}^\dagger \hat{a}_{\nu\mathbf{k}-\mathbf{q}}^\dagger$. Neutral excited states can be generated via the use of optical perturbations, such as laser pulses, if the frequency of the pulse is tuned in resonance to the absorption peaks in the bound region of the spectrum of a material.

The interest in the physics of the excitons grew significantly in recent years, for both fundamental and technological reasons. On one side, the development of femtosecond laser pulses made it possible to explore ultrafast electron dynamics, with the exciton playing a key role due to the optical nature of the perturbation [4–7]. Different works have discussed the possible generation of excitonic states and in particular of nonequilibrium Bose-Einstein condensate (BEC) of excitons [8–13]. On the technological side, the growing interest in materials for applications to photovoltaic devices and semiconductor devices calls for accurate modeling of the absorption process and the interaction between electrons and holes which, in turn, strongly affects carriers mobility. Many new materials, in particular layered materials such as transition metal dichalcogenides [14–16], and chromium or bismuth trihalide [17,18], display remarkably high binding energy for semiconductors. When studied through pump and probe experiments, such materials are often driven via laser pulses

tuned resonant with such excitonic energies. The transient absorption (TR-abs) or the time-resolved angle-resolved photoemission (TR-ARPES) signals are then detected [19–23]. It is then crucial to have accurate modeling and understanding of both the state generated by the pump and the signal measured by the probe.

Due to the coherent nature of the laser pulse, the system is sent into coherent superpositions of the ground state and neutral excitations, which is usually referred to as “coherent excitons.” Many works in the literature have been focused on the description of such experiments [24–26] modeling coherent excitons, either as an ideal boson or via a parametric Wannier equation [12,27,28]. On the other hand, in the *ab initio* community the modeling of such experiments has focused on a detailed description of the material properties and the photoexcitation process, but somehow neglecting the role of the electron-hole interaction and thus describing the generated nonequilibrium density in terms of free carriers. The main reason behind this is the intrinsic difficulty in a fully *ab initio* modeling of excitons in the nonequilibrium regime. Time-dependent density functional theory (TDDFT), the workhorse for *ab initio* nonequilibrium dynamics [29,30], cannot easily capture the physics of the exciton [31,32]. The recent attempts to go beyond TDDFT, within *ab initio* nonequilibrium (NEQ) many-body perturbation theory (MBPT) have, so far, not accounted for the physics of the exciton in the description of the probed signal [33–36]. As a consequence, the interpretation of an experimental signal has seen the use of different concepts, sometimes reaching completely different conclusions [26,27,33–35].

The goal of the present work is to close this gap and model fully *ab initio* the transient signal, taking into account the role of the electron-hole interaction in both the pumping process and the probe process. I will use LiF as a prototype material which displays a strongly bound exciton [37], and consider the physical regime where (i) the pump and the probe do not overlap in time, and (ii) the pump pulse is tuned resonant to the absorption of LiF, thus generating a real NEQ population. Moreover, a low pump pulse intensity is used to

*davide.sangalli@ism.cnr.it

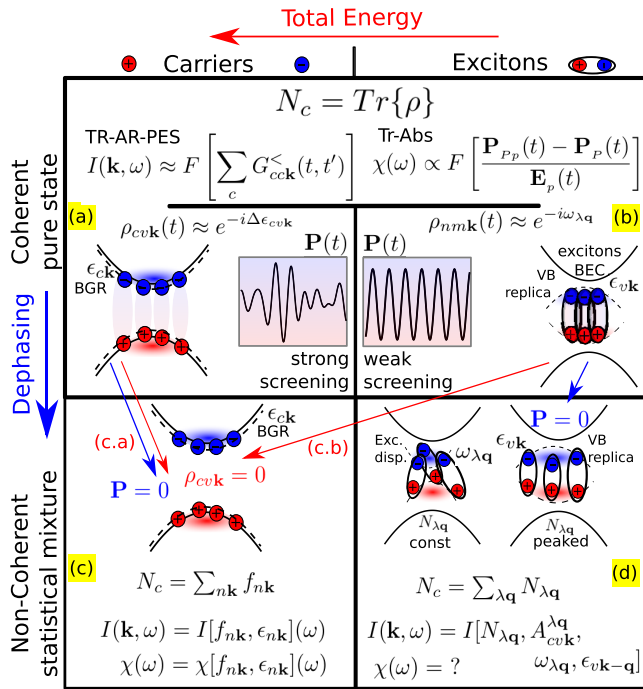


FIG. 1. Overview of the four nonequilibrium states considered in the present work. They are divided into free carriers and bound exciton states (left to right), and in coherent pure states and noncoherent statistical mixtures (top to bottom). N_c is the excited density in the conduction band. The equations used to reconstruct the TR-ARPES spectral function $I(\mathbf{k}, \omega)$ and the response function $\chi(\omega)$ are sketched in the top. In the bottom the approximation used in the literature and holding for the noncoherent case are also reported. The graphical representation of the states is realized via their TR-ARPES signal.

remain below the exciton Mott transition [38,39]. I emphasize that the scheme used in the present work could be also employed in other physical regimes, for example, to describe the overlapping regime, where the dynamical Stark effect plays a key role [8,40], and in the case where the pump is tuned off-resonant (i.e., with a frequency below the optical gap) leading to the generation of a transient virtual NEQ population and of the Floquet replica [41]. This is, however, beyond the goal of the present work.

II. COHERENT AND NONCOHERENT STATES

In Fig. 1 an overview of the physical states considered in the present work is shown. I will use the labels of the panels in this figure to identify these states in the paper: (a) for coherent carriers, (b) for coherent excitons, (c.a) for noncoherent carriers obtained dephasing the coherent carriers state, (c.b) for noncoherent carriers obtained via artificial dephasing of the coherent exciton state, and (d) for noncoherent excitons obtained via physical dephasing of the excitonic state. Physical and artificial dephasing are represented via blue and red lines, respectively, in the figure. Their meaning will be discussed in the paper. The two processes are identical and lead to the same state in the presence of free carriers, while they must

be distinguished and lead to different states in the presence of bound excitons.

The states are generated via the propagation of the equation of motion (EOM) for the time-dependent density matrix $\rho_{nmk}(t)$ in the presence of a pump field. The Hartree plus screened exchange approximation (HSEX), with the screening kept frozen at equilibrium, is used for the many-body self-energy entering the EOM [42]. No further approximation is introduced.

$$i\partial_t \rho_{nmk} = \Delta \epsilon_{nmk} \rho_{nmk} + [\Delta \Sigma^{HSEX}, \rho]_{nmk} + [U^{ext}, \rho]_{nmk}. \quad (1)$$

Starting from $\rho_{nmk}(t)$, I reconstruct the TR-ARPES and the Tr-Abs signal. The TR-ARPES spectral function $I(\mathbf{k}, \omega)$ in the conduction region is obtained via a Fourier transform of $G_{cc'k}^<(t, t')$ [43], with $G_{nmk}^<(t, t')$ reconstructed from $\rho_{nmk}(t)$ using the generalized Kadanoff-Baym ansatz, which is exact within the chosen approximation. The Tr-Abs signal $\chi(\omega)$ is extracted via the Fourier transform of the time-dependent polarization $\mathbf{P}(t) = \mathbf{P}_{Pp}(t) - \mathbf{P}_p(t)$ obtained performing one simulation with only the pump pulse and another with both the pump and the probe pulse, as already discussed in the literature [44,45]. In both cases, the signal depends on the time window used to perform the Fourier transform which, in turn, depends on the probe pulse delay τ from the pump and the decay of $\mathbf{P}_p(t)$. The τ dependence in the equations is omitted since I focus on the transient signal due to the states generated right after the action of the pump pulse. The signal extracted from such coherent states will be compared with the signal generated from a noncoherent population of carriers f_{nk} or excitons $N_{\lambda q}$. The update of the screening is neglected also in the definition of the transient signal. The reason for this choice is twofold. (i) I want to stick to the HSEX approximation with equilibrium screening in all the steps. (ii) I aim for a clear comparison between the signal generated in the excitonic case, with the signal generated in the carriers' case. In the excitonic case, the update of the screening is expected to be negligible in the low-density regime [9,46], i.e., below the exciton Mott transition density. Above such density excitons evaporate, going through a BCS-like regime of electrons and holes [10,25] and it is not meaningful anymore to speak about "excitonic case." In the case of free carriers there exists also a Mott transition density (this has been studied in doped silicon, for example [47]) above which the carriers become a metallic gas and the screening update could easily become the dominant contribution, washing out a possible detailed comparison of other effects. Thus the results presented here are meaningful for densities below both such Mott transitions. As shown in Fig. 2, LiF absorption is dominated by a peak of excitonic nature at about 12.5 eV with a binding energy of almost 2 eV. Two possible frequencies, ω_p , are then considered for the pump laser pulse used: (i) $\omega_{p_a} = 14.8$ eV above the band gap of LiF, and (ii) $\omega_{p_b} = 12.5$ eV resonant to the lowest excitonic peak of LiF (see Fig. 2). The laser pulse is introduced in the form of an oscillating function centered at the pump energy, multiplied by a Gaussian which determines the pulse duration: $\sin(\omega_p t) e^{-(t-t_0)^2/2\sigma^2}$. Here I use $\sigma = 10$ fs. The laser tuned in the continuum generates free carriers with an associated polarization (see Fig. 1, left panel). In this regime, the electron-hole interaction has a negligible

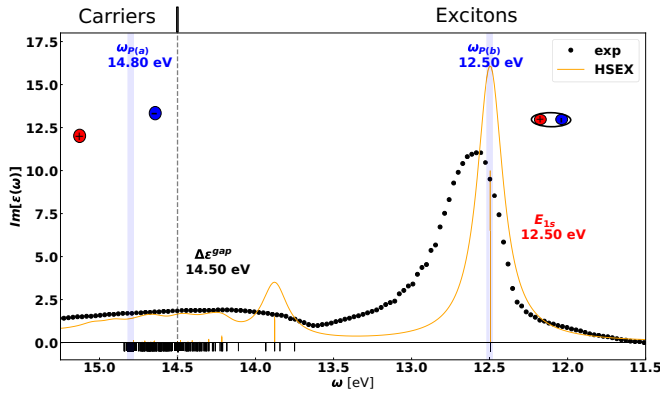


FIG. 2. The optical absorption of LiF. Vertical lines mark the position of the bright eigenvalues of the BSE equation weighted by the associated oscillator strength in the positive y axis. The full BSE spectrum is represented in the negative y axis. The vertical dashed lines represent the position of the electron-hole continuum, i.e., the GW band gap. All the BSE eigenvalues at lower energy are part of the Rydberg exciton series.

effect. The propagation at the independent-particles (IP) level is a good approximation to the TD-HSEX scheme, and it overcomes convergence issues [48]. The laser-tuned resonant with the excitonic peak generates a coherent excitonic state with an associated polarization [see Fig. 1(b)]. The two time propagations are performed for 160 fs. The propagation of the EOM thus generates the two coherent states of Fig. 1.

Dephasing is expected to take place and eventually lead to a statistical mixture of states for carriers [Fig. 1(c)] or excitons [Fig. 1(d)]. For noninteracting electrons, i.e., at the IP level, the most natural way to produce a statistical mixture via the EOM for $\rho(t)$ is to introduce a dephasing term, $-\eta\rho_{nmk}$ for $\{nm\}$ such that $\Delta\epsilon_{nm} > \epsilon_{\text{thresh}}$. This kills the elements of the density matrix that display coherent oscillations, and it produces a state which is time independent. The remaining elements of the density matrix can be interpreted as the nonequilibrium electronic occupations: $f_{nk} = \rho_{nmk}$. The described dephasing procedure corresponds to a real dephasing process in the case of free carriers. Indeed when applied to the coherent carriers state, the IP total energy of the system is conserved. In the presence of interacting electrons instead, such procedure should be performed at the level of the many-body density matrix. For the excitonic case captured at the HSEX level, interacting electron-hole pairs are considered and dephasing could be introduced at the level of the two-body density matrix [49]. Applying the dephasing at the level of the one-body density matrix introduces a change in the total energy of the system, and leads to the formation of carriers populations in place of bound exciton populations. The dephasing term which needs to be introduced in the EOM for $\rho(t)$ to generate a statistical distribution of excitonic population is, however, not known. Two further time propagations are performed, with a dephasing term. Dephasing is switched on after the end of the pump laser pulse at $t = 60$ fs and then switched off at $t = 160$ fs, i.e., before the action of the probe pulse. Since the dephasing acts only after the end of the laser pulse, $\rho_{nmk}^{(a/b)} = \rho_{nmk}^{(c,a/b)}$ (here the superscript refers to the state

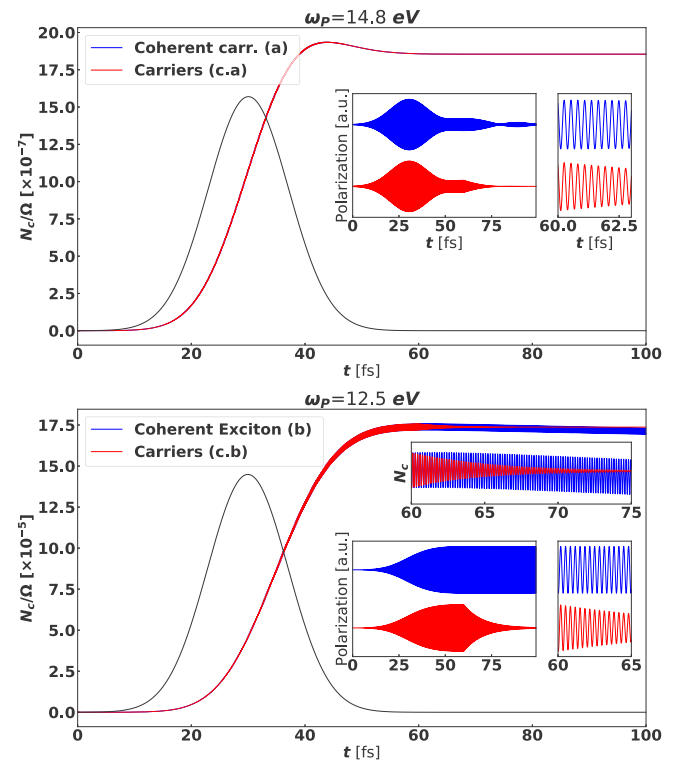


FIG. 3. Time-dependent plot of the total carrier density N_c per unit cell (blue and red lines) and laser pulse intensity profile of the pump (black line) are shown in the main frames. Coherent carriers (a) and noncoherent carriers (c.a) are shown in the upper panel. Coherent exciton (b) and noncoherent carriers distribution obtained dephasing the excitonic state (c.b) in the lower panel. This corresponds to four states introduced in Fig. 1. A zoom of the carrier density N_c is shown in the uppermost inset for the excitonic case. All other insets show the associated time-dependent polarization in different time ranges.

label). With this procedure, two extra states are produced. We refer to (c.a) as the state obtained from the dephasing of the coherent carriers state (a), and to (c.b) as the state obtained from the dephasing of the coherent excitons state (b).

Thus in summary I have generated four states after 160 fs of simulation corresponding to the states (a) and (c.a), and (b) and (c.b) for Fig. 1. In Fig. 3 the total excited density $N_c(t) = \sum_{ck} \rho_{ck}(t)$ and the polarization $\mathbf{P}(t) = e \sum_{n \neq mk} \rho_{nmk}(t)$ of LiF for these four states are shown. The Gaussian envelope of the laser pulse is also shown. The polarization of the coherent carriers state contains a continuum of frequencies and experiences free polarization decay (FPD) on a very short timescale. Here the FPD is not complete due to the finite k -points sampling. On the other hand, in the coherent excitons case, a single frequency exists, and the polarization is everlasting. This already suggests that the role of the coherent oscillations in the spectrum is expected to be more important in the excitonic case. For each state, I further propagate the EOM without any dephasing term from $t = 160$ fs to $t = 200$ fs, first without and later with a probe pulse. A delta function at $t = 165$ fs is used for the probe pulse.

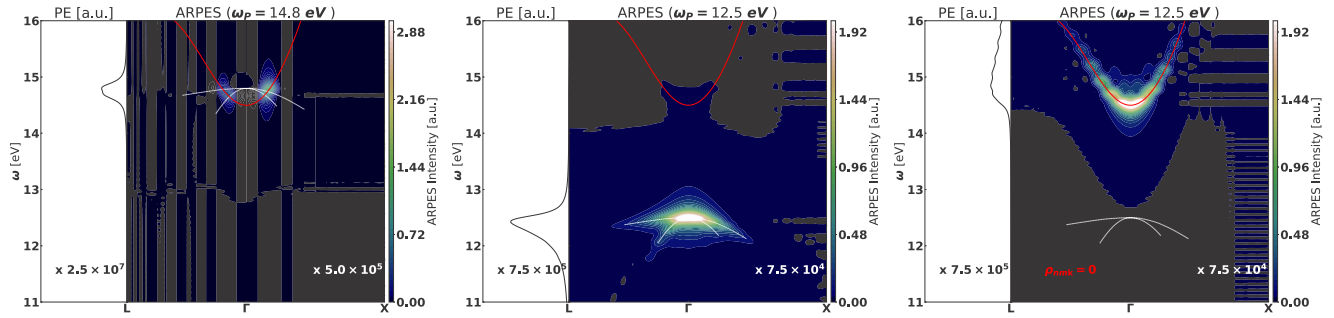


FIG. 4. TR-ARPES spectral function, and corresponding \mathbf{k} -integrated photoemission (PE) signal of LiF. Left panel: Signal from carriers generated with a laser pulse with $\omega_p = 14.8$ eV; coherent (a) and noncoherent (c.a) carriers give exactly the same signal. Center panel: Signal from coherent excitons (b) generated with a laser pulse with $\omega_p = 12.5$ eV. Right panel: Signal from the carriers distribution reached, starting from the coherent exciton state, after sending to zero the off-diagonal elements of the density matrix (c.b). A replica of the valence band at energy $\epsilon_{v\mathbf{k}} + \omega_p$ is shown in white. The numbers reported in the PE and ARPES panels represent the magnification factor needed for the signal in the conduction band region to reach similar intensity as the signal from the valence band (see also Supplemental Material [48]).

III. TIME-RESOLVED ARPES

We first analyze the TR-ARPES signal, shown in Fig. 4 for the four states generated. The spectral function is defined from the time propagation without probe pulse as $I(\mathbf{k}, \omega) = -i \sum_{cc'} G_{cc'\mathbf{k}}^<(\omega)$, obtained via the Fourier transform of the Generalized Kadanoff-Baym Ansatz (GKBA) Green's function [50]

$$G_{cc'\mathbf{k}}^<(t, t') = \sum_n \rho_{cn\mathbf{k}}(t) G_{nc'\mathbf{k}}^{(r)}(t, t') - G_{cn\mathbf{k}}^{(a)}(t, t') \rho_{nc'\mathbf{k}}(t'). \quad (2)$$

The TR-ARPES spectral function generated from free carriers, after the pump at $\omega_{p_a} = 14.8$ eV, shows a finite signal on the conduction band of LiF (see Fig. 4, left panel). The same numerical result can be obtained at the TD-HSEX level (see Supplemental Material [48]). At the IP level the retarded and advanced propagators remain frozen at the equilibrium value and are diagonal: $G_{nm\mathbf{k}}^{(r/a)}(t, t') = \delta_{n,m} e^{-i\epsilon_{n\mathbf{k}}(t-t')}$. As a consequence only the terms $\rho_{cc'\mathbf{k}}$ enter Eq. (2). Since we have here just one conduction band well separated from the others, the ARPES signal from the coherent carriers state (a) and the dephased carriers (a.c) are in practice identical. In the figure it is also reported a replica of the valence band shifted up by 14.8 eV (i.e., the pump frequency). The ARPES signal is localized where the valence band (VB) replica crosses the conduction band, thus for the $\{v_{p_a}, c_{p_a}, \mathbf{k}_{p_a}\}$ which respect the energy conservation at the IP level $\omega_p = \epsilon_{c\mathbf{k}} - \epsilon_{v\mathbf{k}}$. The same signal can be obtained expressing the TR-ARPES in terms of the occupations only $I(\mathbf{k}, \omega) = \sum_c f_{c\mathbf{k}} \delta(\omega - \epsilon_{c\mathbf{k}})$. This result can be easily obtained from Eq. (2) using the IP expression for the retarded and advanced propagators and the definition of the electronic populations in terms of the diagonal elements of the density matrix. In the presence of nearly degenerate conduction bands (i.e., when $\Delta\epsilon_{cc'} \leq 2\pi/\sigma$), $\rho_{c \neq c'\mathbf{k}}$ terms may be activated and have important implications in specific cases. As an example, $\rho_{c \neq c'\mathbf{k}}$ terms have key importance in defining the spin-resolved (SR) TR-ARPES signal of free carriers injected via optical orientation experiments in GaAs [51].

The TR-ARPES spectral function generated from the coherent exciton state (b), after the pump at $\omega_{p_a} = 12.5$ eV, is instead a replica of the valence band shifted by the exciton energy and weighted by the exciton wave function (see Fig. 4, center panel). In this configuration the TD-HSEX retarded and advanced propagators, $G_{nm\mathbf{k}}^{(r/a)}(t, t')$, reconstructed from the time-ordered exponential of the HSEX Hamiltonian, acquire nondiagonal terms which, multiplied by the fast oscillating $\rho_{nm\mathbf{k}}(t)$ terms, determine the TR-ARPES signal. For the coherent exciton state generated by the pump pulse, in the low-density regime, an exact expression can be derived for $G^<(t, t')$ exploiting the mapping between the state generated by the pump pulse and the state generated via the Matsubara procedure discussed in Ref. [10]:

$$G_{cc'\mathbf{k}}^<(\omega) = (2\pi i) N_c \sum_v A_{cv\mathbf{k}}^{\lambda_1 0} A_{c'\mathbf{k}}^{\lambda_1 0,*} \delta[\omega - (\epsilon_{v\mathbf{k}-\mathbf{q}} + \omega_{\lambda\mathbf{q}})]. \quad (3)$$

Such expression perfectly describes the signal obtained via the real-time propagation and shown in Fig. 4, center panel. The state corresponds to an exciton population peaked at the lowest energy exciton $\{\lambda_1 \mathbf{0}\}$, i.e., $N_{q\lambda} = N_{\text{exc}} \delta_{\lambda\lambda_1} \delta(\mathbf{q})$, with $E_{\lambda_1 \mathbf{0}} = 12.5$ eV. Due to its coherent nature, it is referred to as nonequilibrium exciton BEC. The prefactor determining the intensity of the signal corresponds to the mean [52] value of the excitonic population $N_{\text{exc}} = N_c$ [9,10]. The TR-ARPES spectral function generated from the noncoherent state (c.b), after sending to zero the off-diagonal elements of the density matrix, is reported in Fig. 4, right panel, and it is *completely different* from that of the center panel which also includes the off-diagonal terms of the density matrix. After the dephasing, the signal has contribution only from the conduction band, while its distribution in k space is reminiscent from the excitonic wave function $A_{cv\mathbf{k}}^{\lambda_1 0}$. Indeed it can be shown that $f_{c\mathbf{k}} = \rho_{c\mathbf{k}} \propto \sum_v |A_{cv\mathbf{k}}^{\lambda_1 0}|^2$. Such drastic change proves the unphysical nature of the chosen decoherence procedure, which completely alters the state generated by the pump pulse.

As we already observed, it is nontrivial to define a proper dephasing process within the EOM for the one-body density matrix ρ which leads to an exciton population [Fig. 1(d)].

The reason is that the exciton is a two-particle object and approximations to its description can be more easily obtained starting from the two-body density matrix [49]. Nevertheless, the ARPES signal predicted from a noncoherent excitonic population has been discussed in the literature. The signal has the form [53]

$$I[N_{\lambda\mathbf{q}}](\mathbf{k}, \omega) = 2\pi \sum_{\lambda\mathbf{q}\mathbf{c}} N_{\lambda\mathbf{q}} |A_{c\nu\mathbf{k}}^{\lambda\mathbf{q}}|^2 [\omega - (\epsilon_{\nu\mathbf{k}-\mathbf{q}} + \omega_{\lambda\mathbf{q}})]. \quad (4)$$

In the limit of a peaked excitonic distribution $N_{\mathbf{q}\lambda} \approx N_{\text{exc}} \delta_{\lambda\lambda'} \delta(\mathbf{q})$, again a replica of the valence band weighted by the excitonic wave function is obtained. Thus, regardless of originating from a coherent or a noncoherent state, the excitonic ARPES signal has the same shape [10,12]. Recently this feature was exploited to try to measure experimentally the excitonic wave function [54]. As at the IP level, one difference is that in the noncoherent case the terms with $c \neq c'$ are not accounted for. Other differences could be found probing the system with a time resolution short enough to resolve the ultrafast oscillations of the coherent excitonic state [11,39,50]. This, however, would in general lead to loss of energy resolution. The main message of this section is that the ARPES signal of a system with a finite excitonic population has a clear signature [Fig. 4 (b)] and that such signal can be constructed fully *ab initio* within the TD-HSEX scheme.

IV. TRANSIENT ABSORPTION

We now turn to the analysis of the Tr-Abs signal from the four states discussed so far. To this end I compute $\mathbf{P}^{(i)}(t) = \mathbf{P}_{Pp}(t) - \mathbf{P}_p(t)$ obtained from the two time propagations with and without the probe. Again the superscript is a label for the corresponding state: $i = a, c.a, b, c.b$. The probe pulse used is a deltalike function in time which excites the whole spectrum. A dephasing term is applied when the Fourier transform of the polarization is performed to smooth the final result:

$$P^{(i)}(\omega) = \int_{t_p} dt \mathbf{P}^{(a/c.a)}(t) e^{i\omega t - \eta(t-t_p)}. \quad (5)$$

The transient signal is obtained subtracting the equilibrium contribution: $P^{(i)}(\omega) - P^{(eq)}(\omega)$. Following the derivation of Ref. [45], it can be shown that this can be approximated via an adiabatic response function constructed from the nonequilibrium density matrix $\chi[\rho_{nm\mathbf{k}}(\tau)](\omega)$.

In the top panel of Fig. 5, the Tr-Abs generated from the coherent carriers state (a) and noncoherent carriers state (c.a) are compared. The inset shows a plot of the corresponding $P^{(a/c.a)}(\omega)$ polarization. While the pump step can be described at the IP level for the pump resonant with the continuum, in the probing step excitonic effects cannot be neglected. This is why, to construct the Tr-Abs signal, I start from the state generated at the IP level, but I further propagate the EOM in the time window 160–260 fs at the HSEX level. A detailed discussion on this point can be found in the Supplemental Material. Since the EOM is propagated at the HSEX level, the signal corresponds to the adiabatic response function obtained solving the Bethe-Salpeter equation $\chi^{BSE}[\rho_{nm\mathbf{k}}(\tau)](\omega)$. The adiabatic approximation gives the exact result if the time duration of the probe process is much slower than the dynamics

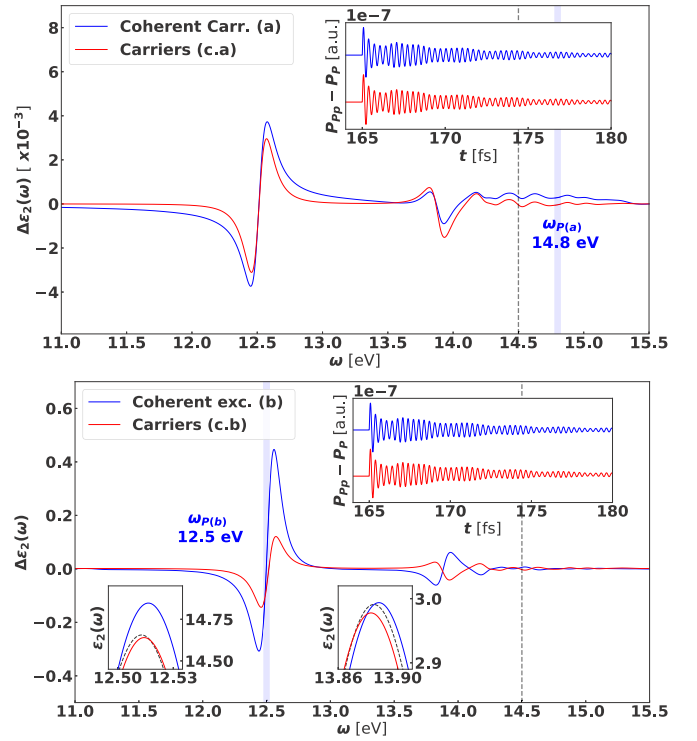


FIG. 5. Transient absorption $\Delta\epsilon_2^{(i)}(\omega) = \epsilon_2^{(i)}(\omega) - \epsilon_2^{(eq)}(\omega)$ for LiF shown for the four states introduced in Fig 1: coherent carriers (a) and noncoherent carriers (c.a), and coherent exciton (b) and noncoherent carriers distribution obtained dephasing the excitonic state (c.b). The probe-induced polarization $\mathbf{P}^{(i)}(t) = \mathbf{P}_{Pp}(t) - \mathbf{P}_p(t)$ is shown in the inset. The blue shaded line marks the laser pump frequency, and the black dashed line the position of the quasiparticle gap. The two extra insets in the lower panel show a zoom of $\epsilon_2^{(i)}(\omega)$ (black line) and $\epsilon_2^{(eq)}(\omega)$ around the two main excitonic peaks.

of the density matrix. This is the case in the noncoherent carriers state (c.a), where the density matrix is time independent. The adiabatic formulation offers a clear interpretation of the transient signal: due to the nonequilibrium density matrix, on one side there is a reduction or bleaching of the transition due to Fermi blocking, and on the other side both the quasiparticle energies and the excitonic energies are renormalized [55]. This explains the overall derivative signal, which is dominated by the energies renormalization, especially in the bound region. In the coherent carriers state (a), corrections due to the time oscillating terms $\rho_{n \neq m\mathbf{k}}(t)$ exist (as opposed to the TR-ARPES signal of the system driven in the continuum). However, they give here a negligible contribution as shown in Fig. 5.

In the bottom panel of Fig. 5 the Tr-Abs generated from the coherent exciton state (b) and the noncoherent state (c.b) are compared. The inset shows a plot of the corresponding $P^{(b/c.b)}(\omega)$ polarization. While in the noncoherent case the signal can be interpreted via the adiabatic response function $\chi^{BSE}[\rho_{nm\mathbf{k}}(\tau)](\omega)$, in the coherent case (b) the adiabatic approximation is not justified, because there is a dominant fast oscillation in $\rho_{n \neq m\mathbf{k}}(t)$. To analyze the transient absorption signal we can inspect the EOM for $\rho_{c\nu\mathbf{k}}$, Eq. (1). The term involving the variation of the HSEX self-energy can

be expanded to linear order in the probe, i.e., I take either the self-energy, $\Delta\Sigma^{Hxc,P}$, or the density matrix, ρ_{cvk}^P , evaluated without the presence of the probe. As discussed in the Supplemental Material, these two terms give rise to a renormalization of the excitonic peaks. Finally, the term $[U^{ext}, \rho]_{cvk}$ can be seen as the source of bleaching, or more in general of changes in the intensity of the peaks. This explains (without the need of the adiabatic approximation) the derivative signal at the excitonic energies shown in Fig. 5. Both for the coherent excitonic state (b) and the noncoherent carriers state (c.b) the signal is mostly localized nearby the pumping energy $\omega_{p_b} = 12.5$ eV, due to a blueshift of the excitonic peak at 12.5 eV. The similarity between the signal of the two states (b) and (c.b) is in sharp contrast with the TR-ARPES case, where the dephasing procedure completely changed the nature of the signal. The reason is twofold. In TR-ARPES (i) the electron-hole interaction has a negligible role in the interaction of the probe pulse with the system since the probe does not generate excitons. However, (ii) the signal is directly affected by the excitons generated by the pump pulse since the exciton binding energy must be supplied to break them and extract carriers. On the other hand, in the Tr-Abs case (i) the probe generates coherent excitonic states in the energy window of 12.5 eV and the electron-hole interaction has a key role in this process, and (ii) the signal is only indirectly affected by the presence of the excitons generated by the pump pulse. Nevertheless, some differences between the carriers and the coherent exciton case remain. At the lowest energy excitonic peak, at 12.5 eV, the peak intensity is reduced for the noncoherent state (c.b), while it is enhanced for the coherent excitonic state (b). The effect on the peak around 14.0 eV is even more striking with an opposite shift in the two cases.

We now try to define the expected signal for the noncoherent excitonic state (d), starting from the excitonic operators, $\hat{e}_{\lambda\mathbf{q}}^\dagger, \hat{e}_{\lambda\mathbf{q}}$, and use a noninteracting boson approximation, i.e., assuming that (i) the excitonic operator follows the bosonic commutation rules and that (ii) the energy needed to generate an exciton is independent of the exciton population. Doing so I also neglect terms where the probe promotes an existing exciton to a higher energy state. Such transition ($\omega_{\lambda\mathbf{q}} - \omega_{\lambda'\mathbf{q}}$) requires one to consider the internal structure of the exciton, and is expected to be important in the low-energy range of the spectrum [6]. The BSE response function can be defined starting from the (retarded) excitonic propagator

$$L_{\lambda\lambda'}^{BSE}(\omega) = \delta_{\lambda\lambda'} \left(\frac{1 + N_{\lambda\mathbf{0}}}{\omega - \omega_{\lambda\mathbf{0}} + i\eta} - \frac{N_{\lambda\mathbf{0}}}{\omega - \omega_{\lambda\mathbf{0}} + i\eta} \right), \quad (6)$$

which is independent on the excitonic population. Indeed the emission term, proportional to $N_{\lambda\mathbf{0}}$, is exactly compensated by the enhancement of the absorption term due to the factor $1 + N_{\lambda\mathbf{0}}$. I mention that, on the contrary, time-resolved photoluminescence (TR-PL) experiments can be well described starting from the bosonic approximation to the exciton [9] since only the emission term is needed. The BSE response function $\chi^{BSE}(\omega)$ constructed from $L_{\lambda\lambda'}^{BSE}(\omega)$ is identical to the equilibrium one. This means that, while in TR-ARPES

the signal can be modeled, as a first approximation, starting from the bosonic nature of the exciton, in Tr-Abs the same approximation gives zero signal, and the corrections to the bosonic nature of the exciton need to be considered. This is why in Fig. 1(d) there is no expression for $\chi^{BSE}[N_{\lambda\mathbf{q}}](\omega)$. Nevertheless, the above analysis gives us some hints. The absence of bleaching is in contrast with what would happen in the presence of free carriers populations, where both the emission term [proportional to $f_{c\mathbf{k}}(1 - f_{v\mathbf{k}})$] and the absorption term [proportional to $f_{v\mathbf{k}}(1 - f_{c\mathbf{k}})$] are bleached due to Pauli blocking. Indeed, as we observed looking at the numerical results, the excitonic peaks are bleached in the presence of carriers, while they are enhanced in the presence of coherent excitons. The results presented in the present paper show that also in Tr-Abs experiments the signal due to carriers and excitons can be distinguished, although the effect is less striking than the TR-ARPES case. A more detailed analysis is needed to further clarify this point, including a scheme able to compute numerically the Tr-Abs from a noncoherent excitonic state.

V. CONCLUSION

In conclusion, I presented a scheme to describe pump and probe experiments including the physics of the exciton. The approach has been implemented in the real-time module of the YAMBO code [56], and tested both in the case where LiF is driven in resonance with the excitonic state and in the case where the pump energy is in the continuum. The results highlight the importance of excitonic effects first of all in the TR-ARPES case, but also in the description of Tr-Abs experiments. Part of the discussion has been focused on the transition from a coherent state to a noncoherent population. Recently published results, based on the interpretation of pump and probe experiments via *ab initio* simulations that do not fully account for excitonic effects, could be reviewed [33–36]. The approach can become the reference scheme to describe the generation and the detection of coherent excitons in a wide range of materials, in the same way the *ab initio* Bethe-Salpeter equation becomes the reference scheme for modeling excitons at equilibrium. Different extensions are possible, including the update of the screening to capture the exciton Mott transition at higher pump fluences or the inclusion of the interaction with phonons and photons to properly model the dynamics of the coherent state, exciton dephasing processes, and exciton lifetimes [57–60].

ACKNOWLEDGMENTS

I acknowledge funding from Ministero dell'Istruzione, dell'Università e della Ricerca MIUR (Italy), PRIN Grant No. 20173B72NB, from the European Union, project MaX Materials design at the eXascale H2020-EINFRA-2015-1 (Grant Agreement No. 824143), and project Nanoscience Foundries and Fine Analysis-Europe H2020-INFRAIA-2014-2015 (Grant Agreement No. 654360).

- [1] G. D. Mahan, Excitons in degenerate semiconductors, *Phys. Rev.* **153**, 882 (1967).
- [2] G. Onida, L. Reining, and A. Rubio, Electronic excitations: Density-functional versus many-body Green's-function approaches, *Rev. Mod. Phys.* **74**, 601 (2002).
- [3] S. Albrecht, L. Reining, R. Del Sole, and G. Onida, *Ab Initio* Calculation of Excitonic Effects in the Optical Spectra of Semiconductors, *Phys. Rev. Lett.* **80**, 4510 (1998).
- [4] S. K. Sundaram and E. Mazur, Inducing and probing non-thermal transitions in semiconductors using femtosecond laser pulses, *Nat. Mater.* **1**, 217 (2002).
- [5] C. Manzoni, O. D. Mücke, G. Cirimi, S. Fang, J. Moses, S.-W. Huang, K.-H. Hong, G. Cerullo, and F. X. Kärtner, Coherent pulse synthesis: Towards sub-cycle optical waveforms, *Laser Photonics Rev.* **9**, 129 (2015).
- [6] S. W. Koch, M. Kira, G. Khitrova, and H. M. Gibbs, Semiconductor excitons in new light, *Nat. Mater.* **5**, 523 (2006).
- [7] J. Chemla and D. S. Shah, Many-body and correlation effects in semiconductors, *Nature (London)* **411**, 549 (2001).
- [8] S. Schmitt-Rink, D. S. Chemla, and H. Haug, Nonequilibrium theory of the optical Stark effect and spectral hole burning in semiconductors, *Phys. Rev. B* **37**, 941 (1988).
- [9] S. A. Moskalenko and D. W. Snoke, *Bose-Einstein Condensation of Excitons and Biexcitons: And Coherent Nonlinear Optics with Excitons* (Cambridge University Press, Cambridge, UK, 2000).
- [10] E. Perfetto, D. Sangalli, A. Marini, and G. Stefanucci, Pump-driven normal-to-excitonic insulator transition: Josephson oscillations and signatures of BEC-BCS crossover in time-resolved ARPES, *Phys. Rev. Mater.* **3**, 124601 (2019).
- [11] A. Rustagi and A. F. Kemper, Coherent excitonic quantum beats in time-resolved photoemission measurements, *Phys. Rev. B* **99**, 125303 (2019).
- [12] D. Christiansen, M. Selig, E. Malic, R. Ernstorfer, and A. Knorr, Theory of exciton dynamics in time-resolved ARPES: Intra- and intervalley scattering in two-dimensional semiconductors, *Phys. Rev. B* **100**, 205401 (2019).
- [13] C. Triola, A. Pertsova, R. S. Markiewicz, and A. V. Balatsky, Excitonic gap formation in pumped Dirac materials, *Phys. Rev. B* **95**, 205410 (2017).
- [14] D. Y. Qiu, F. H. da Jornada, and S. G. Louie, Optical Spectrum of MoS₂: Many-Body Effects and Diversity of Exciton States, *Phys. Rev. Lett.* **111**, 216805 (2013).
- [15] A. Molina-Sánchez, D. Sangalli, K. Hummer, A. Marini, and L. Wirtz, Effect of spin-orbit interaction on the optical spectra of single-layer, double-layer, and bulk MoS₂, *Phys. Rev. B* **88**, 045412 (2013).
- [16] M. Manca, M. M. Glazov, C. Robert, F. Cadiz, T. Taniguchi, K. Watanabe, E. Courtade, T. Amand, P. Renucci, X. Marie, G. Wang, and B. Urbaszek, Enabling valley selective exciton scattering in monolayer WSe₂ through upconversion, *Nat. Commun.* **8**, 14927 (2017).
- [17] A. Molina-Sánchez, G. Catarina, D. Sangalli, and J. Fernández-Rossier, Magneto-optical response of chromium trihalide monolayers: Chemical trends, *J. Mater. Chem. C* **8**, 8856 (2020).
- [18] S. Mor, V. Gosetti, A. Molina-Sánchez, D. Sangalli, S. Achilli, V. F. Agekyan, P. Franceschini, C. Giannetti, L. Sangaletti, and S. Pagliara, Photoinduced coherent modulation of an excitonic resonance via coupling with coherent optical phonons [Phys. Rev. Lett. (to be published)], [arXiv:2105.12587](https://arxiv.org/abs/2105.12587).
- [19] A. Stolow, A. E. Bragg, and D. M. Neumark, Femtosecond time-resolved photoelectron spectroscopy, *Chem. Rev.* **104**, 1719 (2004).
- [20] H. Ueba and B. Gumhalter, Theory of two-photon photoemission spectroscopy of surfaces, *Prog. Surf. Sci.* **82**, 193 (2007).
- [21] U. Bovensiepen and P. Kirchmann, Elementary relaxation processes investigated by femtosecond photoelectron spectroscopy of two-dimensional materials, *Laser Photonics Rev.* **6**, 589 (2012).
- [22] C. L. Smallwood, R. A. Kaindl, and A. Lanzara, Ultrafast angle-resolved photoemission spectroscopy of quantum materials, *Europhys. Lett.* **115**, 27001 (2016).
- [23] J. K. Freericks, H. R. Krishnamurthy, and T. Pruschke, Theoretical Description of Time-Resolved Photoemission Spectroscopy: Application to Pump-Probe Experiments, *Phys. Rev. Lett.* **102**, 136401 (2009).
- [24] K. Henneberger, G. Manzke, V. May, and R. Zimmermann, Nonequilibrium Green's functions and kinetic equations for highly excited semiconductors: II. application to the study of nonlinear optical and transport properties of the many-exciton system, *Phys. A* **138**, 557 (1986).
- [25] L. Kappei, J. Szczytko, F. Morier-Genoud, and B. Deveaud, Direct Observation of the Mott Transition in An Optically Excited Semiconductor Quantum Well, *Phys. Rev. Lett.* **94**, 147403 (2005).
- [26] G. Berghäuser, I. Bernal-Villamil, R. Schmidt, R. Schneider, I. Niehues, P. Erhart, S. Michaelis de Vasconcellos, R. Bratschitsch, A. Knorr, and E. Malic, Inverted valley polarization in optically excited transition metal dichalcogenides, *Nat. Commun.* **9**, 971 (2018).
- [27] C. Trovatiello, F. Katsch, N. J. Borys, M. Selig, K. Yao, R. Borrego-Varillas, F. Scotognella, I. Kriegel, A. Yan, A. Zettl, P. J. Schuck, A. Knorr, G. Cerullo, and S. D. Conte, The ultrafast onset of exciton formation in 2D semiconductors, *Nat. Commun.* **11**, 5277 (2020).
- [28] E. Malic, M. Selig, M. Feierabend, S. Brem, D. Christiansen, F. Wendler, A. Knorr, and G. Berghäuser, Dark excitons in transition metal dichalcogenides, *Phys. Rev. Mater.* **2**, 014002 (2018).
- [29] U. De Giovannini, G. Brunetto, A. Castro, J. Walkenhorst, and A. Rubio, Simulating pump-probe photoelectron and absorption spectroscopy on the attosecond timescale with time-dependent density functional theory, *ChemPhysChem* **14**, 1363 (2013).
- [30] U. De Giovannini, H. Hübener, and A. Rubio, A first-principles time-dependent density functional theory framework for spin and time-resolved angular-resolved photoelectron spectroscopy in periodic systems, *J. Chem. Theory Comput.* **13**, 265 (2017).
- [31] L. Reining, V. Olevano, A. Rubio, and G. Onida, Excitonic Effects in Solids Described by Time-Dependent Density-Functional Theory, *Phys. Rev. Lett.* **88**, 066404 (2002).
- [32] A. Marini, R. Del Sole, and A. Rubio, Bound Excitons in Time-Dependent Density-Functional Theory: Optical and Energy-Loss Spectra, *Phys. Rev. Lett.* **91**, 256402 (2003).
- [33] E. A. A. Pogna, M. Marsili, D. D. Fazio, S. D. Conte, C. Manzoni, D. Sangalli, D. Yoon, A. Lombardo, A. C. Ferrari, A. Marini, G. Cerullo, and D. Prezzi, Photo-induced bandgap renormalization governs the ultrafast response of single-layer MoS₂, *ACS Nano* **10**, 1182 (2016).

- [34] V. Smejkal, F. Libisch, A. Molina-Sanchez, C. Trovatello, L. Wirtz, and A. Marini, Time-dependent screening explains the ultrafast excitonic signal rise in 2D semiconductors, *ACS Nano* **15**, 1179 (2021).
- [35] Z. Wang, A. Molina-Sánchez, P. Altmann, D. Sangalli, D. De Fazio, G. Soavi, U. Sassi, F. Bottegoni, F. Ciccacci, M. Finazzi, L. Wirtz, A. C. Ferrari, A. Marini, G. Cerullo, and S. Dal Conte, Intravalley spin-flip relaxation dynamics in single-layer WS₂, *Nano Lett.* **18**, 6882 (2018).
- [36] A. Molina-Sánchez, D. Sangalli, L. Wirtz, and A. Marini, *Ab initio* calculations of ultrashort carrier dynamics in two-dimensional materials: Valley depolarization in single-layer WSe₂, *Nano Lett.* **17**, 4549 (2017).
- [37] A. Marini and A. Rubio, Electron linewidths of wide-gap insulators: Excitonic effects in LiF, *Phys. Rev. B* **70**, 081103(R) (2004).
- [38] S. W. Koch, W. Hoyer, M. Kira, and V. S. Filinov, Exciton ionization in semiconductors, *Phys. Status Solidi B* **238**, 404 (2003).
- [39] E. Perfetto, S. Bianchi, and G. Stefanucci, Time-resolved ARPES spectra of nonequilibrium excitonic insulators: Revealing macroscopic coherence with ultrashort pulses, *Phys. Rev. B* **101**, 041201(R) (2020).
- [40] S. Schmitt-Rink and D. S. Chemla, Collective Excitations and the Dynamical Stark Effect in a Coherently Driven Exciton System, *Phys. Rev. Lett.* **57**, 2752 (1986).
- [41] U. D. Giovannini and H. Hübener, Floquet analysis of excitations in materials, *J. Phys.: Mater.* **3**, 012001 (2019).
- [42] C. Attaccalite, M. Grüning, and A. Marini, Real-time approach to the optical properties of solids and nanostructures: Time-dependent Bethe-Salpeter equation, *Phys. Rev. B* **84**, 245110 (2011).
- [43] E. Perfetto, D. Sangalli, A. Marini, and G. Stefanucci, First-principles approach to excitons in time-resolved and angle-resolved photoemission spectra, *Phys. Rev. B* **94**, 245303 (2016).
- [44] S. A. Sato, K. Yabana, Y. Shinohara, T. Otake, and G. F. Bertsch, Numerical pump-probe experiments of laser-excited silicon in nonequilibrium phase, *Phys. Rev. B* **89**, 064304 (2014).
- [45] E. Perfetto, D. Sangalli, A. Marini, and G. Stefanucci, Nonequilibrium Bethe-Salpeter equation for transient photoabsorption spectroscopy, *Phys. Rev. B* **92**, 205304 (2015).
- [46] E. Perfetto, A. Marini, and G. Stefanucci, Self-consistent screening enhances the stability of the nonequilibrium excitonic insulator phase, *Phys. Rev. B* **102**, 085203 (2020).
- [47] K. Jain, S. Lai, and M. V. Klein, Electronic Raman scattering and the metal-insulator transition in doped silicon, *Phys. Rev. B* **13**, 5448 (1976).
- [48] See Supplemental Material at <http://link.aps.org/supplemental/10.1103/PhysRevMaterials.5.083803> for a detailed comparison of TD-IP and TD-HSEX when the system is driven in the continuum.
- [49] D. Sangalli, E. Perfetto, G. Stefanucci, and A. Marini, An *ab-initio* approach to describe coherent and non-coherent exciton dynamics, *Eur. Phys. J. B* **91**, 171 (2018).
- [50] This definition of the TR-ARPES signal implicitly assumes that the time resolution is longer than the fast oscillations at the frequency of the exciton, and accordingly the terms $G_{\text{cvk}}^<(t, t')$ can be neglected. This is a necessary condition if one wants to keep energy resolution in the spectral signal. If the probe pulse is short enough then $\{t, t'\} \rightarrow t_{\text{probe}}$ and one is left with an energy integrated signal which oscillates in time as discussed in Refs. [10,11].
- [51] M. D'Alessandro and D. Sangalli, Real-time modeling of optical orientation in GaAs: Generation and decay of the degree of spin polarization, *Phys. Rev. B* **102**, 104437 (2020).
- [52] A coherent state is not an eigenstate of the population operator, thus we can only speak about the mean excitonic population.
- [53] A. Rustagi and A. F. Kemper, Photoemission signature of excitons, *Phys. Rev. B* **97**, 235310 (2018).
- [54] S. Dong, M. Puppini, T. Pincelli, S. Beaulieu, D. Christiansen, H. Hübener, C. W. Nicholson, R. P. Xian, M. Dendzik, Y. Deng, Y. W. Windsor, M. Selig, E. Malic, A. Rubio, A. Knorr, M. Wolf, L. Rettig, and R. Ernstorfer, Direct measurement of key exciton properties: Energy, dynamics, and spatial distribution of the wave function, *Nat. Sci.* **1**, e10010 (2021).
- [55] D. Sangalli, S. Dal Conte, C. Manzoni, G. Cerullo, and A. Marini, Nonequilibrium optical properties in semiconductors from first principles: A combined theoretical and experimental study of bulk silicon, *Phys. Rev. B* **93**, 195205 (2016).
- [56] D. Sangalli, A. Ferretti, H. Miranda, C. Attaccalite, I. Marri, E. Cannuccia, P. Melo, M. Marsili, F. Paleari, A. Marrazzo, G. Prandini, P. Bonfà, M. O. Atambo, F. Affinito, M. Palummo, A. Molina-Sánchez, C. Hogan, M. Grüning, D. Varsano, and A. Marini, Many-body perturbation theory calculations using the YAMBO code, *J. Phys.: Condens. Matter* **31**, 325902 (2019).
- [57] M. Palummo, M. Bernardi, and J. C. Grossman, Exciton radiative lifetimes in two-dimensional transition metal dichalcogenides, *Nano Lett.* **15**, 2794 (2015).
- [58] F. Paleari, H. P. C. Miranda, A. Molina-Sánchez, and L. Wirtz, Exciton-Phonon Coupling in the Ultraviolet Absorption and Emission Spectra of Bulk Hexagonal Boron Nitride, *Phys. Rev. Lett.* **122**, 187401 (2019).
- [59] P. Cudazzo, First-principles description of the exciton-phonon interaction: A cumulant approach, *Phys. Rev. B* **102**, 045136 (2020).
- [60] H.-Y. Chen, D. Sangalli, and M. Bernardi, Exciton-Phonon Interaction and Relaxation Times from First Principles, *Phys. Rev. Lett.* **125**, 107401 (2020).